minerals

MDPI

Article

Effect of Al_2O_3 on Sound Velocity of $MgSiO_3$ Glass at High Pressure

Xinmiao Wei [1,†], Lingling Dong [1,†], Fangfei Li [1], Qiang Zhou [1,2], Caizi Zhang [1], Mengqi Guo [1], Yingzhan Wei [1], Xue Zhang [1], Liang Li [1], Xinyang Li [1,*] and Zhaodong Liu [1,2]

1 State Key Laboratory of Superhard Materials, College of Physics, Jilin University, Changchun 130012, China
2 Synergetic Extreme Condition User Facility, Jilin University, Changchun 130012, China
* Correspondence: lixinyang@jlu.edu.cn
† These authors contributed equally to this work.

Abstract: Silicate glass has been used as an analog for silicate melts to understand the nature of dense magmas in the Earth's mantle. To understand the effect of Al_2O_3 on the sound velocity and structure of $MgSiO_3$ glass, in this study, combined with Brillouin scattering and diamond anvil cells (DACs), the acoustic velocity of $MgSiO_3$·5 mol%Al_2O_3 (MA1) and $MgSiO_3$·24.5 mol%Al_2O_3 (MA2) glass were measured up to 20 and 42 GPa, respectively. Our studies show that the incorporation of Al_2O_3 could increase the sound velocity of $MgSiO_3$ glass. Using the obtained velocities, the bulk and shear moduli (K_S, G), density (ρ) and Poisson's ratio (ν) are calculated at high pressures, and the results indicate that Al_2O_3 could induce the stiffness of $MgSiO_3$ glass. However, the effect of Al_2O_3 content on the stiffness of $MgSiO_3$ glass is non-linear, and MA1 and MA2 exhibit similar K_S and G at high pressures. With the increase of pressure, the transverse acoustic mode (V_S) of MA1 and MA2 shows abnormal changes at 17.8 GPa and 31.8 GPa, which are related to the transition of coordination number (CN) for Si-O in Al-bearing $MgSiO_3$ glass. Compared with previous studies on sound velocity of $MgSiO_3$ glass, the incorporation of Al_2O_3 delays the transition pressure of Si-O coordination to a higher pressure. Our study has profound implications for understanding the density and sound velocity of Al-bearing $MgSiO_3$ melt in the Earth's interior.

Keywords: Brillouin scattering; high pressure; sound velocity; $MgSiO_3$-Al_2O_3 glass

check for updates

Citation: Wei, X.; Dong, L.; Li, F.; Zhou, Q.; Zhang, C.; Guo, M.; Wei, Y.; Zhang, X.; Li, L.; Li, X.; et al. Effect of Al_2O_3 on Sound Velocity of $MgSiO_3$ Glass at High Pressure. *Minerals* **2022**, *12*, 1069. https://doi.org/10.3390/min12091069

Academic Editors: Yann Morizet and Leonid Dubrovinsky

Received: 29 June 2022
Accepted: 23 August 2022
Published: 24 August 2022

1. Introduction

Seismic data have observed many low velocity zones at the Earth's upper mantle [1], transition zone [2] and core mantle boundary [3], which might be related to the melting or partial melting of silicates. However, due to the limitation of techniques, static experimental studies on physicochemical properties of silicate melts are only investigated at relatively low pressure by large volume presses [4–7]. To overcome the limitations, theoretical calculations can be used to determine the properties of silicate melts at the whole conditions of the Earth's interior [8–10]. In addition, silicate glass is commonly used as an analog to study the physicochemical properties of silicate melts at high pressure and temperature [11,12]. Thus, investigation on the high-pressure behaviors of silicate glass, such as sound velocity, structural transition and equation of state helps increase understanding of the properties of melt at high pressures [11,13,14].

$MgSiO_3$, as the most abundant component in the Earth's mantle, is present as pyroxene and bridgmanite in the Earth's upper and lower mantle, respectively. The structural and elastic properties of $MgSiO_3$ glass were investigated by X-ray absorbance, optical laser Raman, X-ray Raman scattering and Brillouin scattering at high pressures [12,14–17]. These studies indicate that $MgSiO_3$ glass undergoes a local structural change at the Mg site below 10 GPa and a Si-O coordination number (CN) change above 15.9 GPa [13–17]. Al_2O_3 is one of the most important components in the Earth's mantle, and the Al_2O_3 contents in

pyrolite bulk mantle and in the basalt layer of subducted oceanic lithosphere range between 4 and 16 wt.% [18,19]. The Al_2O_3 solubility in bridgmanite is up to 29 mol.% at 52 GPa [20]. However, to date, only one study investigated the structure and sound velocity of pyrope ($Mg_3Al_2Si_3O_{12}$) glass below 12.9 GPa [21], and thus the effect of Al_2O_3 on the physical properties of $MgSiO_3$ glass needs further investigation at higher pressures. In this study, considering the Al_2O_3 content in the Earth's interior, we investigated the sound velocity of $MgSiO_3$ glass with two different Al_2O_3 contents up to 20 and 42 GPa. The results indicate that the incorporation of Al_2O_3 makes $MgSiO_3$ glass stiffer. The substitution of Al in the Si site could delay the transition of Si-O CN to higher pressure. The results have profound implications for understanding the behavior of silicate melts in the Earth's lower mantle.

2. Experiments

$MgSiO_3$·5 mol%Al_2O_3 (MA1) and $MgSiO_3$·24.5 mol%Al_2O_3 (MA2) were prepared from oxide mixtures of reagent-grade MgO, SiO_2, and Al_2O_3 in 19:19:1 (MA1) and 3:3:1 (MA2) mole ratio. The starting materials were fused at 2000 K for 1 h, and then quenched into cold water. All the glasses were confirmed to have the intended chemical composition within the analytical uncertainties by using electron microprobe analysis (EMPA, JEOL Superprobe JXA-8230, JEOL Ltd., Jilin University (JLU), Changchun, China) and transmission electron microscopy (TEM, JEOL JEM-2200FS instrument, 200 kV, JEOL Ltd., JLU, Changchun, China) (Table 1). The morphology and homogeneity of those glasses were confirmed by scanning electron microscope (SEM, Philips FEI Quanta Magellan 400, Philips, JLU, Changchun, China), which was equipped with backscattered electron (BSE, the resolution is ~10 nm) (Figure 1). The density of the glass was measured by the Archimedes method [22], and the density was 2.75 and 2.81 g/cm^3 for MA1 and MA2 at ambient condition, respectively.

Table 1. Element compositions of $MgSiO_3$·5 mol%Al_2O_3 and $MgSiO_3$·24.5 mol%Al_2O_3 by electron microprobe analysis.

Element \ Sample	**$MgSiO_3$·5 mol%Al_2O_3 ($Mg_{0.95}Al_{0.1}Si_{0.95}O_3$)**	**$MgSiO_3$·24.5 mol%Al_2O_3 ($Mg_{0.76}Al_{0.49}Si_{0.76}O_3$)**
MgO	38.1(1)	30.3(1)
Al_2O_3	5.1(1)	24.7(1)
SiO_2	56.8(1)	45.2(1)
Mg	0.95(2)	0.76(2)
Al	0.101(3)	0.49(1)
Si	0.95(2)	0.76(1)
O	3.00(6)	3.00(6)
Mg/Si	1	1

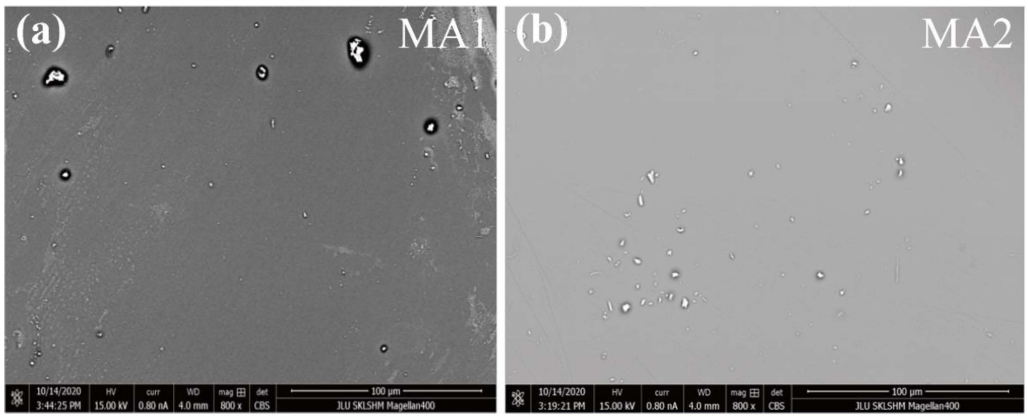

Figure 1. Backscattered electron images of $MgSiO_3$-Al_2O_3 glass: (**a**) MA1; (**b**) MA2. The features on the surface are caused by the surface contamination when preparing the samples.

In situ high-pressure Brillouin scattering measurements of acoustic velocity were performed at room temperature in a BX-90 DAC [23] by using a solid-state laser as an incident light (532 nm) and a Sandercock-type six-pass tandem Fabry–Perot interferometer to analyze the scattered light. The incident laser was focused on the sample to a spot size of ~50 μm in diameter. The laser power was maintained at 0.3 and 0.5 W at room condition and high pressure, respectively. All measurements were made in the symmetric scattering geometry, and the velocities were calculated by the following equation without knowing the refractive index of the sample [24]:

$$v = \frac{\Delta\omega\lambda}{2\sin(\theta/2)} \quad (1)$$

where v is the acoustic velocity, λ is the laser wavelength of the incident laser beam and θ is the external scattering angle; $\Delta\omega$ indicates the Brillouin frequency shifts of longitudinal or transverse acoustic modes. The external scattering angle is 60°.

The glass was polished to a platelet with parallel sides and a thickness of 20 μm and the samples were cut into 90 × 90 μm^2 and loaded into the DACs. A Rhenium gasket was pre-indented to 40 μm in thickness, and with a hole of 190 μm in diameter at the center of indentation that was used as the sample chamber. Because the noble gases with small molecular size, for example, He and Ne, could be incorporated into the structure of glass [25,26], we thus used argon as the pressure-transmitting medium. The sample was compressed with a 300 μm diamond culet. In each experiment, two ruby spheres were loaded next to the sample and were used as a pressure calibrant [27]. To stabilize the pressure, the DACs were kept for one night after increasing the pressure. Pressure was measured before and after Brillouin scattering measurements, and the pressure difference was within 0.2 GPa. We collected Brillouin spectra from at least two rotation angles at each pressure and confirmed the uniformity and isotropy of the samples. The difference of sound velocity was lower than 1% at different rotation angles at the same pressure. MA1 and MA2 were measured up to 20 and 42 GPa, respectively.

3. Results and Discussion

Both V_P and V_S for MA1 and MA2 can be observed in our Brillouin scattering measurements (Figure 2). However, the V_P are masked by the V_S of above 20 GPa, while the V_S of MA1 and MA2 between 4–8 GPa are also blocked by the V_P of Ar. The measured V_P and V_S of MA1 and MA2 as a function of pressure are shown in Figure 3 and Table 2. MA1 and MA2 have basically the same V_P and V_S within the uncertainties (Figure 3). Using the obtained sound velocities, the density (ρ), bulk modulus (K_S), shear modulus (G) and Poisson's ratio (ν) of MA1 and MA2 were calculated at high pressures (Figure 4; Table 2).

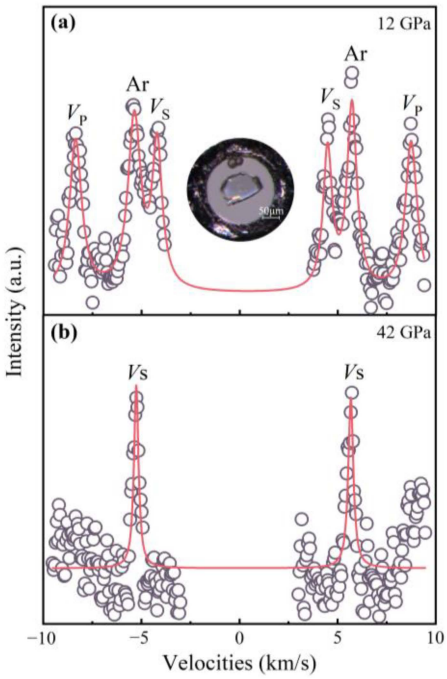

Figure 2. High-pressure Brillouin spectra of MA2 at (**a**) 12 GPa and (**b**) 42 GPa. Compressional V_P and shear V_S wave velocities of $MgSiO_3$-Al_2O_3 glass are labeled, as well as the compressional velocities of Argon (Ar). The open circles are experimental data, solid lines are the fitting result. The insert in (**a**) shows the sample in chamber of DAC.

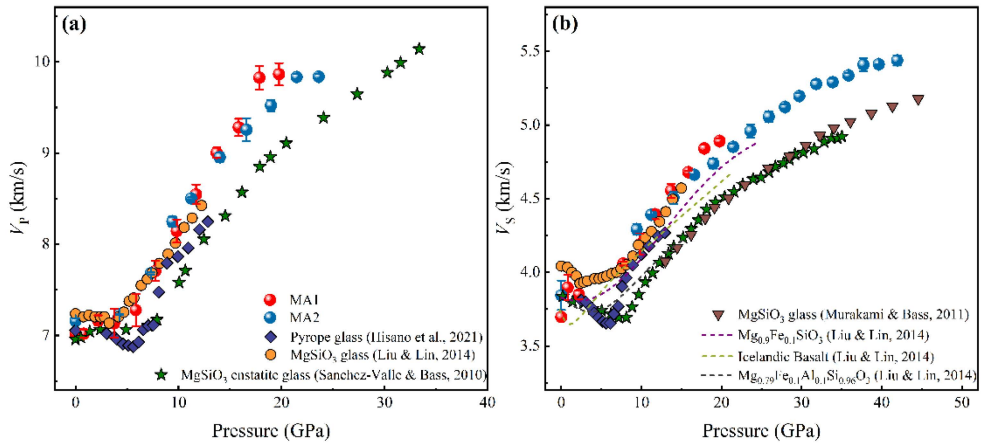

Figure 3. (**a**) V_P as a function of pressure up to 42 GPa. (**b**) V_S as a function of pressure up to 42 GPa. MA1, red filled circles; MA2, blue filled circles. The green pentagrams and blue rhombuses indicate the results of $MgSiO_3$ enstatite glass and pyrope glass from Sanchez-Valle and Bass [14] and Hisano et al. [21], respectively. The orange circles and gray inverted triangles indicate the results of $MgSiO_3$ glass from Liu and Lin [12] and Murakami and Bass [13]. Dashed purple, green and gray lines are non-linear fits to the data for $Mg_{0.9}Fe_{0.1}SiO_3$, Icelandic Basalt and $Mg_{0.79}Fe_{0.1}Al_{0.1}Si_{0.96}O_3$ from Liu and Lin [12], respectively.

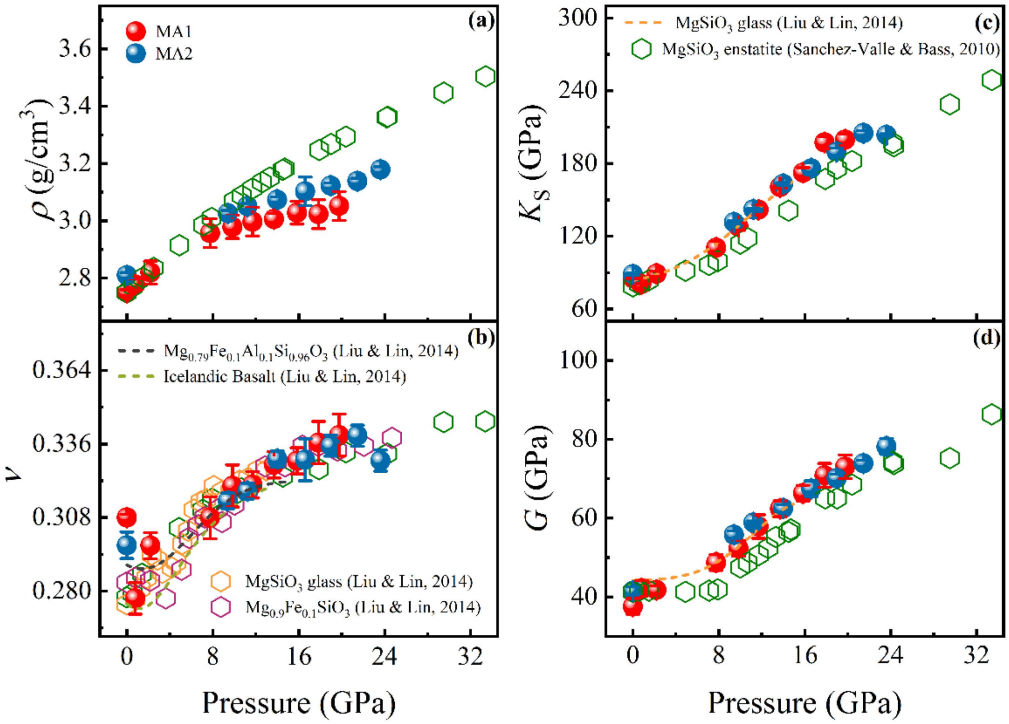

Figure 4. Density (**a**), Poisson's ratio (**b**), bulk (**c**) and shear (**d**) modulus as a function of pressure for $MgSiO_3$-Al_2O_3 glass: MA1 glass, red filled circles; MA2 glass, blue filled circles. The green and orange hollow hexagons indicate the results of $MgSiO_3$ glass from Sanchez-Valle and Bass [14] and Liu and Lin [12], respectively. The purple hollow hexagons indicate the result of $Mg_{0.9}Fe_{0.1}SiO_3$ glass from Liu and Lin [12]. Dashed orange, green and gray lines are non-linear fits to the data for $MgSiO_3$ glass, Icelandic Basalt and $Mg_{0.79}Fe_{0.1}Al_{0.1}Si_{0.96}O_3$ from Liu and Lin [12], respectively.

Table 2. Density and elastic properties of MA1 and MA2 determined up to 20 GPa and 42 GPa using Brillouin scattering in the diamond anvil cell, respectively.

MA1						
Pressure (GPa)	**ρ (g/cm³)**	**V_P (km/s)**	**V_S (km/s)**	**K_S (GPa)**	**G (GPa)**	**ν**
0	2.75(1)	7.02(1)	3.70(1)	85.4(3)	37.5(3)	0.308(1)
0.80	2.78(2)	7.02(5)	3.90(8)	80.6(2)	42(2)	0.277(6)
2.20	2.82(4)	7.17(5)	3.85(3)	89(2)	42(1)	0.298(5)
3.75	-	7.1(2)	-	-	-	-
5.85	-	7.3(2)	-	-	-	-
7.75	2.95(5)	7.7(1)	4.06(1)	111(5)	49(2)	0.308(8)
9.83	2.98(4)	8.2(1)	4.19(7)	128(3)	52(3)	0.320(8)
11.70	3.00(5)	8.6(1)	4.39(3)	142(4)	58(3)	0.321(5)
13.70	3.01(2)	9.01(5)	4.56(5)	160.6(9)	62(2)	0.328(5)
15.85	3.03(4)	9.28(9)	4.68(1)	173(4)	66(2)	0.330(5)
17.85	3.02(5)	9.8(1)	4.84(3)	197(5)	71(3)	0.337(8)
19.76	3.05(5)	9.8(1)	4.89(2)	200(5)	73(3)	0.340(8)
MA2						
Pressure (GPa)	**ρ (g/cm³)**	**V_P (km/s)**	**V_S (km/s)**	**K_S (GPa)**	**G (GPa)**	**ν**
0	2.81(1)	7.16(3)	3.8(1)	89(1)	42(1)	0.298(5)
4.25	-	7.23(1)	-	-	-	-
7.30	-	7.68(1)	-	-	-	-

Table 2. *Cont.*

MA2						
Pressure (GPa)	**ρ (g/cm^3)**	**V_P (km/s)**	**V_S (km/s)**	**K_S (GPa)**	**G (GPa)**	**ν**
9.41	3.03(1)	8.25(5)	4.29(4)	131(1)	56(1)	0.314(3)
11.23	3.05(1)	8.50(1)	4.391(4)	142(1)	58.9(4)	0.318(3)
14	3.07(1)	8.95(5)	4.51(4)	163(1)	63(1)	0.330(3)
16.60	3.10(5)	9.3(1)	4.662(5)	176(5)	68(2)	0.330(8)
18.97	3.12(1)	9.52(6)	4.74(4)	189(3)	70(1)	0.335(4)
21.47	3.14(1)	9.83(3)	4.85(2)	205(2)	73.9(8)	0.339(4)
23.61	3.18(1)	9.84(3)	4.96(5)	203(1)	78(2)	0.330(4)
25.89	-	-	5.06(3)	-	-	-
27.92	-	-	5.12(2)	-	-	-
29.70	-	-	5.20(2)	-	-	-
31.83	-	-	5.28(3)	-	-	-
33.96	-	-	5.29(2)	-	-	-
35.84	-	-	5.34(2)	-	-	-
37.72	-	-	5.41(4)	-	-	-
39.62	-	-	5.411(1)	-	-	-
41.92	-	-	5.44(3)	-	-	-

The densities are calculated by the following equation [14]:

$$\frac{\rho}{\partial P} = \frac{1}{V_B^2}. \tag{2}$$

where $V_B^2 = V_P^2 - \frac{4}{3}V_S^2$. Integrating Equation (2), we obtain:

$$\rho - \rho_0 = \int_{P_0}^{P} \frac{1}{V_B^2} \mathrm{d}P. \tag{3}$$

where ρ and ρ_0 are densities at high pressures (P) and ambient pressure (P_0), respectively. V_B is the bulk sound velocity.

The K_S and G are calculated by the following equation:

$$V_P = \sqrt{\frac{K_S + \frac{4G}{3}}{\rho}}. \tag{4}$$

$$V_S = \sqrt{\frac{G}{\rho}}. \tag{5}$$

where V_P is compressional wave velocity, V_S is shear wave velocity, K_S is the adiabatic bulk modulus, G is the shear modulus and ρ is density.

The Poisson's ratio (ν) is calculated from the acoustic velocities using the following relationship:

$$\nu = \frac{1}{2}\frac{(V_P/V_S)^2 - 2}{(V_P/V_S)^2 - 1}. \tag{6}$$

To compare the sound velocities of different compositional silicate glasses at high pressures, V_P and V_S from different groups are summarized in Figure 3 [12–14]. The results show large discrepancies from different studies (Figure 3) [12–14,21]. Studies indicate that the incorporation of noble gas in the structure of glass could make it stiffer [25,26]. Thus, the pressure mediums need to be considered when comparing the results from different groups. For pure $MgSiO_3$ glass, the velocity of Sanchez-Valle and Bass [14] is in good agreement with Murakami and Bass [13], but lower than the results of Liu and Lin [12]. The discrepancies in the three groups may be due to the different pressure medium used in the

experiments, where Ar was used in Sanchez-Valle and Bass [14], Ne was used in Liu and Lin [12], and no pressure medium was used in Murakami and Bass [13]. Because Ar was also used in our experiment, the results of Sanchez-Valle and Bass [14] can be a reference for understanding the effect of Al_2O_3 on the sound velocity of $MgSiO_3$ glass. In comparison with the results of Sanchez-Valle and Bass [14], the incorporation of 5 mol% Al_2O_3 into $MgSiO_3$ glass increases its V_P and V_S by 6.5–8.3% and 7.4–10% at 10–20 GPa, respectively. In particular, the MA2 exhibits similar sound velocity with MA1, indicating that the additional Al_2O_3 has a small effect on the sound velocity of $MgSiO_3$ glass. In addition, MA2 with a similar composition as used in Hisano et al. [21] shows ~4% and ~5% higher V_P and V_S at high pressures. The large volume press combined with ultrasonic measurements were used in Hisano et al. [21], and the discrepancy should be caused by the uncertainty in different techniques. In particular, compared with different compositional $MgSiO_3$ glass, despite the effect of pressure medium on the sound velocity, the incorporation of Al_2O_3 could substantially enhance the stiffness of $MgSiO_3$ glass (Figure 3).

At the pressure below 10 GPa, Al-free and Al-bearing $MgSiO_3$ glasses have similar density (Figure 4a). However, the pure $MgSiO_3$ glass shows the greatest density above 10 GPa because it has the largest compressibility among these three types of $MgSiO_3$ glass. In addition, the incorporation of Al_2O_3 in the $MgSiO_3$ glass could increase the K_S and G, indicating that Al_2O_3 could induce the stiffness of $MgSiO_3$ glass (Figure 4c,d). However, the effect of Al_2O_3 content on the stiffness should be non-linear at high pressures (Figure 5). The non-linear effect of incorporated element on the stiffness and hardness was also observed in the superhard materials [28–30]. The incorporation of Al_2O_3 in different content would have effects on the valence-electron volumetric density (EVD) and structure of $MgSiO_3$ glass. Thus, MA1 and MA2 exhibit similar K_S and G at high pressures. Compared with the Poisson's ratios with different compositional silicate glass (Figure 4b), MA1 and MA2 show a similar value, indicating that the composition has a limited effect on Poisson's ratios [12].

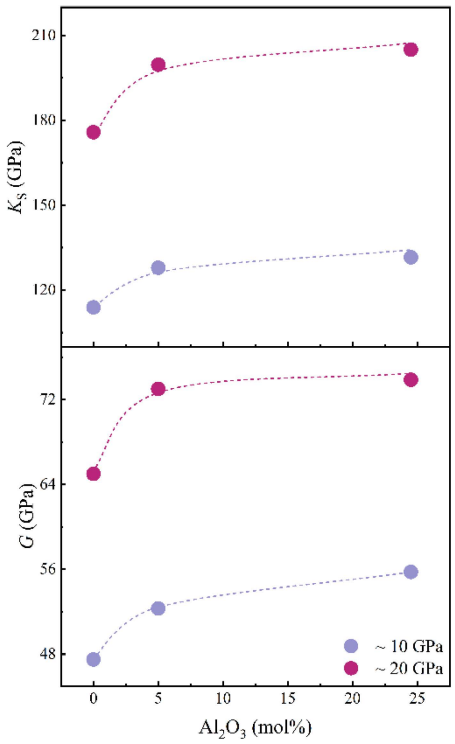

Figure 5. The non-linear relationship between K_S, G and the Al_2O_3 content in $MgSiO_3$-Al_2O_3 glass. Light purple and dark purple solid circles represent the data at the pressures of ~10 and 20 GPa, respectively. The data of pure $MgSiO_3$ glass from Sanchez-Valle and Bass [14].

Overall, the velocities of $MgSiO_3$-type glass have an abnormal change between 2 and 10 GPa (Figure 3). Using magnesium L-edge spectra from XRS, one study indicated that the Mg site in $MgSiO_3$ glass has a distortion and local structural change below 10 GPa, which is consistent with the pressure range of the abnormal change [15]. Another change of gradient in V_S is also reported between 15–17.9 GPa [14] (Figure 3). Both silicon L-edge and oxygen K-edge indicate a change in the CN for Si-O above 10 GPa [15,17]. Thus, the change of gradient in V_S should be caused by the transition of CN of Si-O or the decreasing of Si-O-Si angle [15–17].

To understand the transition of the Si-O polyhedral, the V_S is fitted with a polynomial function to assess the trend change of $MgSiO_3$-Al_2O_3 glass as a function of pressure (Figure 6a). The change of dV_S/dP occurs at 17.8 GPa and 31.8 GPa in MA1 and MA2, respectively, indicating the transition of CN of Si-O from 4 to 5- or 6-fold coordination in the glass [14]. The transition pressure of MA1 is 2 GPa higher than that of $MgSiO_3$ glass [14], and the transition pressure of MA2 is 15 GPa higher than that of $MgSiO_3$ glass (Figure 6b). The results suggested that the incorporation of Al cations delays the transition pressure for the CN of Si-O in $MgSiO_3$ glass.

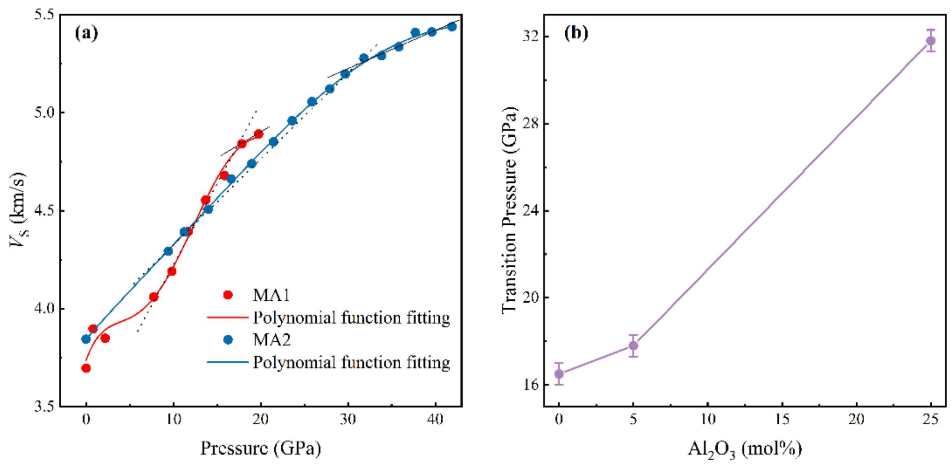

Figure 6. (**a**) P-V_S profiles up to 42 GPa: MA1 (red filled circles), MA2 (blue filled circles). Regression curves of MA1 and MA2 fitted by polynomial functions. P-V_S plots of MA1 from 1 bar to 20 GPa are fitted with a fifth order polynomial (R^2 = 0.9909) and P-V_S plots of MA2 from 1 bar to 42 GPa are fitted with a fifth function (R^2 = 0.9993). (**b**) Transition pressure as a function of the Al_2O_3 content in $MgSiO_3$-Al_2O_3 glass. The pure $MgSiO_3$ glass data are from Sanchez-Valle and Bass [14].

4. Implications

Our sound velocity studies on Al_2O_3-$MgSiO_3$ to lower mantle pressures indicate the effect of Al_2O_3 on the elastic properties and structural changes of $MgSiO_3$ glass. If the change also occurs in the analog melt, it would strongly affect the dynamics of the magma ocean during the Earth's evolution. Density is an important factor for understanding the coexistence between melt and solid phase in the Earth's interior. Previous study indicates that the density of bridgmanite intersected with that of magnesium silicate glass in the deep mantle [14]. However, Al_2O_3 is a critical component in the Earth's interior, and 4–16 wt.% (4.1–16.3 mol.%) Al_2O_3 can be present in the Earth's mantle [18,19]. Our study shows that the density of Al-bearing $MgSiO_3$ glass is much lower than that of Al-bearing bridgmanite [31] (Figure 7). Because of the lower density of Al-bearing $MgSiO_3$ than Al-bearing bridgmanite (Figure 7), Al-bearing $MgSiO_3$ melt tends to upwell and cannot coexist with bridgmanite in the deep Earth's interior. In addition, the incorporation of Al_2O_3 could make the glass stiffer; if this also happens in the analog melt, it will increase the V_P of melt and help to understand the seismic signature of Al-bearing $MgSiO_3$ melt in the Earth's interior.

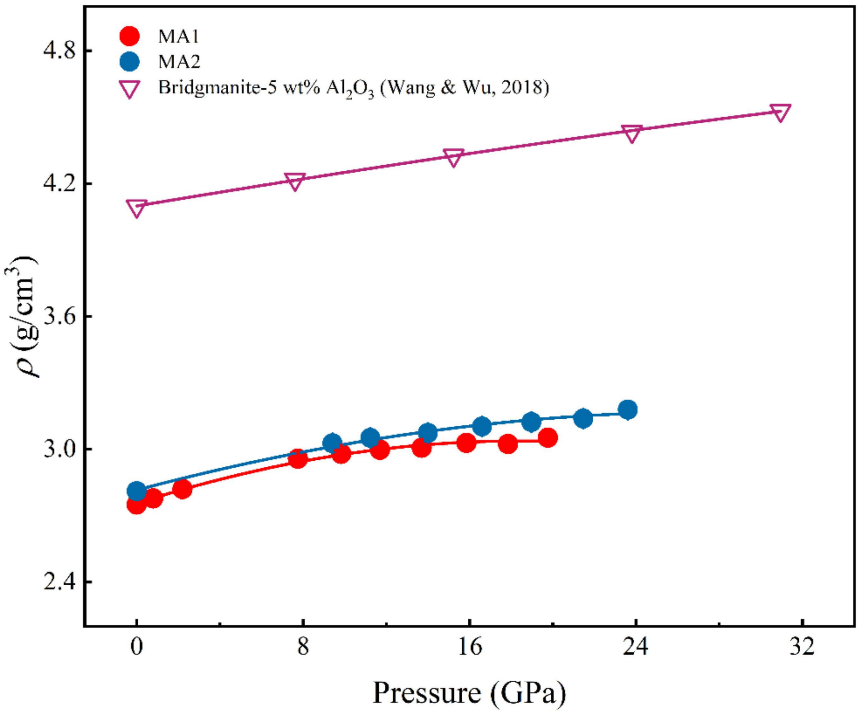

Figure 7. Density as a function of pressure: MA1 (red filled circles), MA2 (blue filled circles). Bridgmanite-5 wt.% Al_2O_3 (purple hollow inverted triangle, Wang and Wu [31]).

5. Conclusions

In summary, the acoustic velocity of $MgSiO_3$ 5 mol%Al_2O_3 (MA1) and $MgSiO_3$·24.5 mol%Al_2O_3 (MA2) glass were measured up to 20 and 42 GPa, respectively. In comparison with pure $MgSiO_3$ glass, Al-bearing $MgSiO_3$ glass exhibited higher velocity, indicating that the incorporation of Al_2O_3 could increase the sound velocity of $MgSiO_3$ glass. Using obtained velocities, the bulk and shear moduli (K_S, G), density (ρ) and Poisson's ratio (ν) of MA1 and MA2 are calculated at high pressures, and the results indicate that Al_2O_3 could induce the stiffness of $MgSiO_3$ glass. However, the effect of Al_2O_3 content on the stiffness of $MgSiO_3$ glass is non-linear, and MA1 and MA2 exhibit similar K and G at high pressures. With the increase of pressure, transverse acoustic modes (V_S) of MA1 and MA2 show abnormal changes at the pressure of 17.8 GPa and 31.8 GPa, which are related to the transition of coordination number (CN) for Si-O in Al-bearing $MgSiO_3$ glass. Compared with previous studies on sound velocity of $MgSiO_3$ glass, the incorporation of Al_2O_3 delays the transition pressure of Si-O coordination to higher pressures. Our study also indicates that the density of Al-bearing $MgSiO_3$ glass is much lower than that of Al-bearing bridgmanite, and the Al-bearing $MgSiO_3$ is unlikely to co-exist with Al-bearing bridgmanite in the Earth's lower mantle.

Author Contributions: X.L. and F.L. conceived and designed the research; Z.L. synthesized the samples; L.D. and X.Z. performed the Brillouin scattering experiments; X.L., X.W. and L.D. analyzed the data; X.L. and X.W. wrote the manuscript; Q.Z. and L.L. funding acquistition, procet administration; Q.Z., C.Z., M.G., Y.W. and L.L. writing—review and editing. All authors have provided very valuable comments on this project. All authors have read and agreed to the published version of the manuscript.

Funding: This research was supported by the China Postdoctoral Science Foundation (2020M670841), the Jilin Provincial Science and Technology Development Project (20210509038RQ), the National Key Research and Development Program (No. 2017YFA0403704) and the National Natural Science Foundation of China (NSFC) (NO. 42102030; 41902034; 12074141).

Data Availability Statement: Data associated with this research are available and can be obtained by contacting the corresponding author.

Conflicts of Interest: The authors declare no conflict of interest.

References

1. Debayle, E.; Bodin, T.; Durand, S.; Ricard, Y. Seismic evidence for partial melt below tectonic plates. *Nature* **2020**, *586*, 555–559. [CrossRef] [PubMed]
2. Song, T.-R.; Helmberger, D.V.; Grand, S.P. Low-velocity zone atop the 410-km seismic discontinuity in the northwestern United States. *Nature* **2004**, *427*, 530–533. [CrossRef] [PubMed]
3. Yuan, K.; Romanowicz, B. Seismic evidence for partial melting at the root of major hot spot plumes. *Science* **2017**, *357*, 393–397. [CrossRef]
4. Agee, C.B. Static compression of hydrous silicate melt and the effect of water on planetary differentiation. *Earth Planet. Sci. Lett.* **2008**, *265*, 641–654. [CrossRef]
5. Huisman, J.; Pham Thi, N.N.; Karl, D.M.; Sommeijer, B. Reduced mixing generates oscillations and chaos in the oceanic deep chlorophyll maximum. *Nature* **2006**, *439*, 322–325. [CrossRef]
6. Xu, M.; Jing, Z.; Yu, T.; Alp, E.E.; Lavina, B.; Van Orman, J.A.; Wang, Y. Sound velocity and compressibility of melts along the hedenbergite ($CaFeSi_2O_6$)-diopside ($CaMgSi_2O_6$) join at high pressure: Implications for stability and seismic signature of Fe-rich melts in the mantle. *Earth Planet. Sci. Lett.* **2022**, *577*, 117250. [CrossRef]
7. Jing, Z.; Yu, T.; Xu, M.; Chantel, J.; Wang, Y. High-Pressure Sound Velocity Measurements of Liquids Using In Situ Ultrasonic Techniques in a Multianvil Apparatus. *Minerals* **2020**, *10*, 126. [CrossRef]
8. Solomatova, N.V.; Caracas, R. Pressure-Induced Coordination Changes in a Pyrolitic Silicate Melt From Ab Initio Molecular Dynamics Simulations. *J. Geophys. Res. Solid Earth* **2019**, *124*, 11232–11250. [CrossRef]
9. Ghosh, D.B.; Karki, B.B. Transport properties of carbonated silicate melt at high pressure. *Sci. Adv.* **2017**, *3*, 1–8. [CrossRef]
10. Wan, J.T.K.; Duffy, T.S.; Scandolo, S.; Car, R. First-principles study of density, viscosity, and diffusion coefficients of liquid $MgSiO_3$ at conditions of the Earth's deep mantle. *J. Geophys. Res. Solid Earth* **2007**, *112*, B03208. [CrossRef]
11. Murakami, M.; Bass, J.D. Spectroscopic Evidence for Ultrahigh-Pressure Polymorphism in SiO_2 Glass. *Phys. Rev. Lett.* **2010**, *104*, 025504. [CrossRef] [PubMed]
12. Liu, J.; Lin, J.-F. Abnormal acoustic wave velocities in basaltic and (Fe,Al)-bearing silicate glasses at high pressures. *Geophys. Res. Lett.* **2014**, *41*, 8832–8839. [CrossRef]
13. Murakami, M.; Bass, J.D. Evidence of denser $MgSiO_3$ glass above 133 gigapascal (GPa) and implications for remnants of ultradense silicate melt from a deep magma ocean. *Proc. Natl. Acad. Sci. USA* **2011**, *108*, 17286–17289. [CrossRef] [PubMed]
14. Sanchez-Valle, C.; Bass, J.D. Elasticity and pressure-induced structural changes in vitreous $MgSiO_3$-enstatite to lower mantle pressures. *Earth Planet. Sci. Lett.* **2010**, *295*, 523–530. [CrossRef]
15. Fukui, H.; Hiraoka, N. Electronic and local atomistic structure of $MgSiO_3$ glass under pressure: A study of X-ray Raman scattering at the silicon and magnesium L-edges. *Phys. Chem. Miner.* **2018**, *45*, 211–218. [CrossRef]
16. Kubicki, J.D.; Hemley, R.J.; Hofmeister, A.M. Raman and infrared study of pressure-induced structural changes in $MgSiO_3$, $CaMgSi_2O_6$, and $CaSiO_3$ glasses. *Am. Mineral.* **1992**, *77*, 258–269.
17. Lee, S.K.; Lin, J.-F.; Cai Yong, Q.; Hiraoka, N.; Eng Peter, J.; Okuchi, T.; Mao, H.-k.; Meng, Y.; Hu Michael, Y.; Chow, P.; et al. X-ray Raman scattering study of $MgSiO_3$ glass at high pressure: Implication for triclustered $MgSiO_3$ melt in Earth's mantle. *Proc. Natl. Acad. Sci. USA* **2008**, *105*, 7925–7929. [CrossRef] [PubMed]
18. Stolper, E. A phase diagram for mid-ocean ridge basalts: Preliminary results and implications for petrogenesis. *Contrib. Mineral. Petrol.* **1980**, *74*, 13–27. [CrossRef]
19. Sun, S.-S. Chemical composition and origin of the earth's primitive mantle. *Geochim. Cosmochim. Acta* **1982**, *46*, 179–192. [CrossRef]
20. Liu, Z.; Irifune, T.; Nishi, M.; Tange, Y.; Arimoto, T.; Shinmei, T. Phase relations in the system $MgSiO_3$–Al_2O_3 up to 52 GPa and 2000 K. *Phys. Earth Planet. Int.* **2016**, *257*, 18–27. [CrossRef]
21. Hisano, N.; Sakamaki, T.; Ohashi, T.; Funakoshi, K.; Higo, Y.; Shibazaki, Y.; Suzuki, A. Elastic properties and structures of pyrope glass under high pressures. *Am. Mineral.* **2021**, *106*, 7–14. [CrossRef]
22. Hughes, S.W. Archimedes revisited: A faster, better, cheaper method of accurately measuring the volume of small objects. *Phys. Educ.* **2005**, *40*, 468–474. [CrossRef]
23. Kantor, I.; Prakapenka, V.; Kantor, A.; Dera, P.; Kurnosov, A.; Sinogeikin, S.; Dubrovinskaia, N.; Dubrovinsky, L. BX90: A new diamond anvil cell design for X-ray diffraction and optical measurements. *Rev. Sci. Instrum.* **2012**, *83*, 125102. [CrossRef] [PubMed]
24. Whitfield, C.H.; Brody, E.M.; Bassett, W.A. Elastic moduli of NaCl by Brillouin scattering at high pressure in a diamond anvil cell. *Rev. Sci. Instrum.* **1976**, *47*, 942–947. [CrossRef]
25. Yang, H.; Gleason, A.E.; Tkachev, S.N.; Chen, B.; Jeanloz, R.; Mao, W.L. Noble gas incorporation into silicate glasses: Implications for planetary volatile storage. *Geochem. Perspect. Lett.* **2021**, *17*, 1–5. [CrossRef]
26. Weigel, C.; Polian, A.; Kint, M.; Rufflé, B.; Foret, M.; Vacher, R. Vitreous Silica Distends in Helium Gas: Acoustic Versus Static Compressibilities. *Phys. Rev. Lett.* **2012**, *109*, 245504. [CrossRef]
27. Mao, H.K.; Xu, J.; Bell, P.M. Calibration of the ruby pressure gauge to 800 kbar under quasi-hydrostatic conditions. *J. Geophys. Res. Solid Earth* **1986**, *91*, 4673–4676. [CrossRef]

28. Liang, Y.; Wei, X.-F.; Gu, C.; Liu, J.-X.; Li, F.; Yan, M.; Zheng, X.; Han, Z.; Zhao, Y.; Wang, S.; et al. Enhanced Hardness in Transition-Metal Monocarbides via Optimal Occupancy of Bonding Orbitals. *ACS Appl. Mater. Interfaces* **2021**, *13*, 14365–14376. [CrossRef]
29. Mohammadi, R.; Turner, C.L.; Xie, M.; Yeung, M.T.; Lech, A.T.; Tolbert, S.H.; Kaner, R.B. Enhancing the Hardness of Superhard Transition-Metal Borides: Molybdenum-Doped Tungsten Tetraboride. *Chem. Mater.* **2016**, *28*, 632–637. [CrossRef]
30. Akopov, G.; Yeung, M.T.; Turner, C.L.; Mohammadi, R.; Kaner, R.B. Extrinsic Hardening of Superhard Tungsten Tetraboride Alloys with Group 4 Transition Metals. *J. Am. Chem. Soc.* **2016**, *138*, 5714–5721. [CrossRef]
31. Wang, W.; Wu, Z. Elasticity of Corundum at High Pressures and Temperatures: Implications for Pyrope Decomposition and Al-Content Effect on Elastic Properties of Bridgmanite. *J. Geophys. Res. Solid Earth* **2018**, *123*, 1201–1216. [CrossRef]